I. Usoltsev, R. Eichler*, Y. Wang, J. Even, A. Yakushev, H. Haba, M. Asai, H. Brand, A. Di Nitto, Ch.E. Düllmann, F. Fangli, W. Hartmann, M. Huang, E. Jäger, D. Kaji, J. Kanaya, Y. Kaneya, J. Khuyagbaatar, B. Kindler, J.V. Kratz, J. Krier, Y. Kudou, N. Kurz, B. Lommel, S. Miyashita, K. Morimoto, K. Morita, M. Murakami, Y. Nagame, H. Nitsche, K. Ooe, T.K. Sato, M. Schädel, J. Steiner, P. Steinegger, T. Sumita, M. Takeyama, K. Tanaka, A. Toyoshima, K. Tsukada, A. Türler, Y. Wakabayashi, N. Wiehl, S. Yamaki, and Z. Qin

Decomposition studies of group 6 hexacarbonyl complexes. Part 1: Production and decomposition of Mo(CO)₆ and W(CO)₆

Abstract: Chemical studies of superheavy elements require fast and efficient techniques, due to short half-lives and low production rates of the investigated nuclides. Here, we advocate for using a tubular flow reactor for assessing the thermal stability of the Sg carbonyl complex – $Sg(CO)_6$. The experimental setup was tested with Mo and W carbonyl complexes, as their properties are established and supported by theoretical predictions. The suggested approach proved to be effective in discriminating between the thermal stabilities of $Mo(CO)_6$ and $W(CO)_6$. Therefore, an experimental verification of the predicted Sg–CO bond dissociation energy seems to be feasible by applying this technique. By investigating the effect of ^{104,105}Mo beta-decay on the formation of ^{104,105}Tc carbonyl complex, we estimated the lower reaction time limit for the metal carbonyl synthesis in the gas phase to be more than 100 ms. We examined further the influence of the wall material of the recoil chamber, the carrier gas composition, the gas flow rate, and the pressure on the production yield of ^{104}Mo(CO)$_6$, so that the future stability tests with $Sg(CO)_6$ can be optimized accordingly.

Keywords: Transition metals, carbonyl complexes, transactinides, group 6, seaborgium, thermal stability.

*Corresponding author: R. Eichler, University of Bern, 3012 Bern, Switzerland; and Paul Scherrer Institute, 5232 Villigen, Switzerland, e-mail: robert.eichler@psi.ch
I. Usoltsev, P. Steinegger, A. Türler: University of Bern, 3012 Bern, Switzerland; and Paul Scherrer Institute, 5232 Villigen, Switzerland
Y. Wang, F. Fangli, Z. Qin: Institute of Modern Physics Lanzhou, Chinese Academy of Sciences, 730000 Lanzhou, China
J. Even: Helmholtz-Institut Mainz, 55099 Mainz, Germany; and recently at TRIUMF, Vancouver, BC V6T 2A3, Canada
J. Khuyagbaatar: Helmholtz-Institut Mainz, 55099 Mainz, Germany; and GSI Helmholtzzentrum für Schwerionenforschung GmbH, 64291 Darmstadt, Germany
N. Wiehl: Helmholtz-Institut Mainz, 55099 Mainz, Germany; and Johannes Gutenberg-Universität Mainz, 55099 Mainz, Germany
Ch.E. Düllmann: Helmholtz-Institut Mainz, 55099 Mainz, Germany; and GSI Helmholtzzentrum für Schwerionenforschung GmbH, 64291 Darmstadt, Germany; and Johannes Gutenberg-Universität Mainz, 55099 Mainz, Germany
A. Yakushev, H. Brand, W. Hartmann, E. Jäger, B. Kindler, J. Krier, N. Kurz, B. Lommel, J. Steiner: GSI Helmholtzzentrum für Schwerionenforschung GmbH, 64291 Darmstadt, Germany

A. Di Nitto, J.V. Kratz: Johannes Gutenberg-Universität Mainz, 55099 Mainz, Germany
H. Haba, M. Huang, D. Kaji, J. Kanaya, Y. Kudou, K. Morimoto, T. Sumita, M. Takeyama, K. Tanaka, Y. Wakabayashi, S. Yamaki: Nishina Center for Accelerator-Based Science, RIKEN, Wako, Saitama 351-0198, Japan
K. Morita: Nishina Center for Accelerator-Based Science, RIKEN, Wako, Saitama 351-0198, Japan; and Kyushu University, Higashi-Ku, Fukuoka, 812-8581, Japan
M. Murakami: Nishina Center for Accelerator-Based Science, RIKEN, Wako, Saitama 351-0198, Japan; and Niigata University, Niigata, Niigata 950-2181, Japan
M. Asai, Y. Kaneya, Y. Nagame, T.K. Sato, M. Schädel, A. Toyoshima, K. Tsukada: Advanced Science Research Center, Japan Atomic Energy Agency, Tokai, Ibaraki 319-1195, Japan
S. Miyashita: Advanced Science Research Center, Japan Atomic Energy Agency, Tokai, Ibaraki 319-1195, Japan; and Hiroshima University, Kagamiyama, Higashi-Hiroshima 739-8526, Japan
K. Ooe: Niigata University, Niigata, Niigata 950-2181, Japan
H. Nitsche: University of California, Berkeley, CA 94720-1460, USA; and Lawrence Berkeley National Laboratory, Berkeley, CA 94720-8169, USA

1 Introduction

Conventional methods for measuring bond dissociation energies of transition metal carbonyls, such as laser pyrolysis [1] are unsuitable when experiments with superheavy elements (SHE, $Z \geq 104$) [2–5] are envisaged. Production rates of a few atoms per hour down to a single atom per months and half-lives shorter than one minute make their chemical characterization rather challenging. However, gas-phase techniques combined with alpha-particle spectroscopy enable a quantitative assessment of chemical properties on a single atomic scale in long-term experiments [6–8]. The synthesis and the adsorption enthalpy (ΔH_{ads}) of the seaborgium hexacarbonyl complex, $Sg(CO)_6$, on a SiO_2 surface have recently been reported [9]. It represents the first chemical characterization of a compound with Sg in its zero oxidation state. The experimental value of ΔH_{ads} was supported by theoretical prediction [10], which included *relativistic effects* [11]. Scaling with Z^2, relativistic effects in the electron structure naturally play an important role in the case of the chemistry of superheavy elements. On the one hand, the contraction of s and $p_{1/2}$ orbitals, referred to as the "*direct relativistic effect*", weakens the σ-donation in the Sg–CO bond. On the other hand, the expansion of d-orbitals, referred to as the "*indirect relativistic effect*", strengthens the contribution of the π-backbonding. The latter effect reinforces the metal-CO bond and is therefore accountable for the expected trend of increasing stability of carbonyl complexes down group 6 of the periodic table. Thus, $Sg(CO)_6$ was predicted to be slightly more stable than the corresponding complex of its lighter homologue – $W(CO)_6$ [12]. The first bond dissociation energy (FBDE) for $Sg(CO)_6$ was calculated to be 197 ± 8 kJ/mol, which is around 4 kJ/mol higher compared to that of $W(CO)_6$ [1].

We consider the production rate of one $Sg(CO)_6$ complex per day, observed in [9], to be sufficient for setting up a thermal stability experiment. A careful design of the setup and an appropriate strategy for carrying out the stability tests are, however, a prerequisite. In this first part of the publication, we focus on the experimental implementation of a future Sg experiment. We use radioactive short-lived isotopes of Mo and W in ultra-trace amounts for testing the suggested setup and to optimize the experimental conditions. The second part [13] addresses the link between the experimental observables presented here and the thermodynamic bond stability in the hexacarbonyl molecules of group 6 elements. Thus, the complete method for a quantitative assessment of the thermal stability of $Sg(CO)_6$ is suggested.

2 Experimental

2.1 Production of $^{104}Mo(CO)_6$

The "Ms. Piggy" ^{252}Cf spontaneous fission (SF) source, installed at the University of Bern, allows for the production of various transition-metal fission products with a wide spread of half-lives [14]. Among the produced Mo isotopes, ^{104}Mo ($T_{1/2} = 60$ s, $E_\gamma = 68.8$ keV, 69.8 keV) [15] is a perfect nuclide for quantifying $Mo(CO)_6$ formation and behavior. Volatile transition-metal carbonyl complexes are formed *in situ* by thermalizing the fission fragments in the recoil chamber (Figure 1), flushed with CO containing carrier gas [16, 17].

2.2 Production of $^{87-88}Mo(CO)_6$ and $^{163-164}W(CO)_6$

For direct comparison between $Mo(CO)_6$ and $W(CO)_6$, both complexes were synthesized at the GAs-filled Recoil Ion Separator (GARIS) [18] at RIKEN, Japan. Two isotopes ^{163}W ($T_{1/2} = 2.6$ s, $E_\alpha = 5.384$ MeV) [19] and ^{164}W ($T_{1/2} = 6$ s, $E_\alpha = 5.150$ MeV) [20] were produced in the heavy-ion induced nuclear fusion reaction $^{144}Sm(^{24}Mg,4\text{-}5n)^{163-164}W$. A rotating target wheel with $^{144}Sm_2O_3$ (251 μg/cm^2), deposited on 3 μm Ti foils, was bombarded by a 0.66 μA$_{part}$ ^{24}Mg beam with an energy of 144 MeV, provided by the RIKEN Linear Accelerator (RILAC). By changing the target material to ^{nat}Zn (natural isotopic abundance, 558 μg/cm^2 thick Zn-foil) and adjusting the ^{24}Mg beam energy to 85 MeV, the isotopes ^{87}Mo ($T_{1/2} = 14.5$ s, $E_\gamma = 263.0$ keV) [21] and ^{88}Mo ($T_{1/2} = 8.2$ min, $E_\gamma = 170.7$ keV) [22] were produced in the reaction $^{nat}Zn(^{24}Mg, xn)^{87,88}Mo$. The recoiling products of the nuclear fusion were separated in GARIS and guided to the focal plane of the separator.
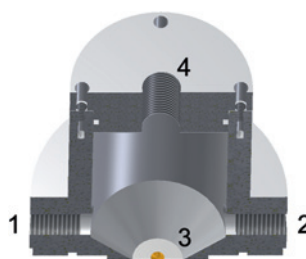
Figure 1: The recoil chamber of the "Ms. Piggy" ^{252}Cf spontaneous fission source. The carrier gas enters the chamber from two inlets (1,2). Fission fragments, recoiling from the ^{252}Cf source (3), are thermalized in the carrier gas, form volatile carbonyl complexes and are finally transported further through the outlet (4).

Here, the products passed through a thin Mylar window separating GARIS from the carrier gas of the chemistry setup. Subsequently, they were thermalized in the CO/He (50 : 50 vol-%) carrier gas flushing through the recoil transfer chamber (RTC). Thus, hexacarbonyl complexes were formed *in situ* [9, 16, 17].

## 2.3 Optimization of the production and transport yields

Volatile carbonyl complexes of fission products formed in the recoil chamber of "Ms. Piggy" were transported and quantitatively retained on a charcoal trap. The activity of the trapped isotopes was monitored by standard γ-ray spectrometry in conjunction with the data acquisition and analysis system Canberra Genie2k®.

Experiments using the Cryo-Online Multidetector for the Physics And Chemistry of Transactinides (COMPACT) [23] determined the amount of the formed and transported $^{163-164}W(CO)_6$. A negative temperature gradient was applied along the thermochromatographic detector array, which ensured the quantitative adsorption and decay of the transported carbonyl complexes within the detector array. Thus, the production and transport yields of $W(CO)_6$ were assessed. In contrast to the energetically discrete alpha-decay of $^{163-164}W$, the β^+-decay of $^{87-88}Mo$ isotopes exhibits a continuous energy spectrum, which precludes an effective distinction between parent and daughter nuclides. For that reason, $^{87-88}Mo(CO)_6$ was collected in the COMPACT detector for 15 min. After stopping the irradiation the decay of $^{87-88}Mo$ isotopes and their daughters were monitored for 15 min. Thereby, the contribution of each of the two Mo isotopes could be clearly assessed due to their distinct half-lives [9]. The combination of physical pre-separation using GARIS and chemical separation by selective formation of carbonyls allowed for an effective separation of the desired evaporation residues from the beam and from byproducts of multinucleon transfer reactions, providing nearly background-free conditions for the measurements [24]. Therefore, the detected beta activity in the COMPACT could be unambiguously assigned to the two Mo isotopes. In addition, the production of $^{87}Mo(CO)_6$ and $^{88}Mo(CO)_6$ was proven in a separate experiment, where both complexes were quantitatively retained on the charcoal trap, which was monitored by a High Purity Germanium (HPGe) γ-ray detector. The detected γ-lines at 263.0 keV and 170.7 keV unequivocally identified ^{87}Mo and ^{88}Mo, respectively.

2.4 Decomposition setup

For the thermal stability tests with the carbonyl compounds, a *decomposition column* was implemented between the recoil chamber and the detection unit (COMPACT or charcoal trap). A scheme of the decomposition setup installed at the "Ms. Piggy" spontaneous fission source is depicted in Figure 2. The experiments at GARIS used a similar implementation: the decomposition column along with the PFA Teflon® bypass of the same size as the decomposition column was installed between the RTC and the COMPACT detector. Otherwise, the gas-loop transport system was used as it is described in [9].

Metal columns (Au, Pd, Ag) were prepared by rolling 25 µm foils (Goodfellow) and inserting them into a quartz tube. The quartz tube with metal foil inserts, was in turn sealed inside a steel tube. Such an arrangement provided a hermetically sealed connection between the decomposition column and the production/detection units. Finally, the steel tube was heated by a resistance furnace (Hillesheim GmbH), connected to a temperature regulator. In the experiments with quartz and PFA Teflon® as materials for the decomposition column, the corresponding decomposition columns were put directly into the resistance furnace. The *decomposition curves* were obtained
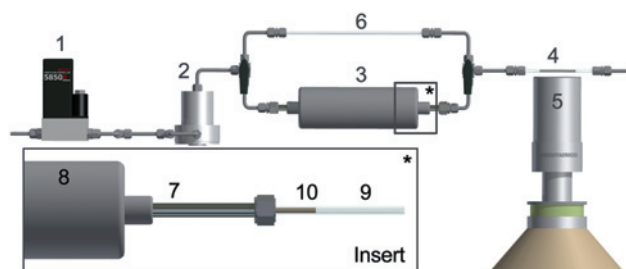
Figure 2: Principal scheme of the setup used for the decomposition studies. Regulated by mass flow controllers (1), gases were mixed before entering the recoil chamber of "Ms. Piggy" spontaneous fission source (2 and Figure 1). The thermalized fission fragments formed volatile compounds, which were flushed out of the chamber into the 1 m long decomposition column (3) and finally, depending on the decomposition rates, reached the charcoal trap (4), where they were quantitatively retained. The activity on the trap was monitored by a HPGe γ-ray detector (5). The decomposition column could be by-passed through a PFA Teflon® column (6), held at room temperature. The exact same geometry, compared to the decomposition column, allowed for measuring undisturbed production rates at given experimental conditions. Insert: sketch of the open decomposition column (3): a stainless steel tube (7) was inserted into a regulated resistance furnace (8). Inside the stainless steel tube there was a quartz column (9), used as a casing for metal foil inserts (10), which thereby formed a *metal column*. All the connectors were based on Swagelok® parts for He-tight hermetical sealing.
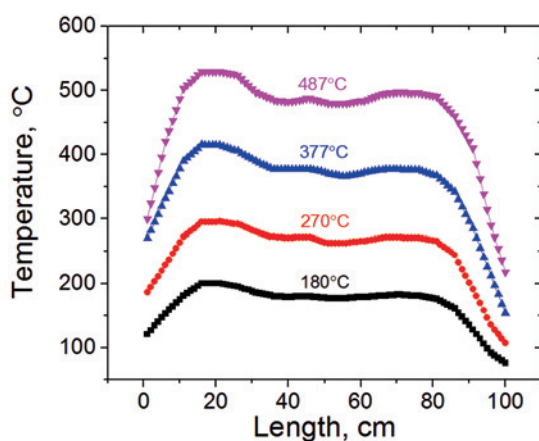
Figure 3: Temperature profiles in the decomposition column determined at different *plateau temperatures*. Plateau temperatures were regulated and monitored in the middle of the furnace and their values are shown above each profile.
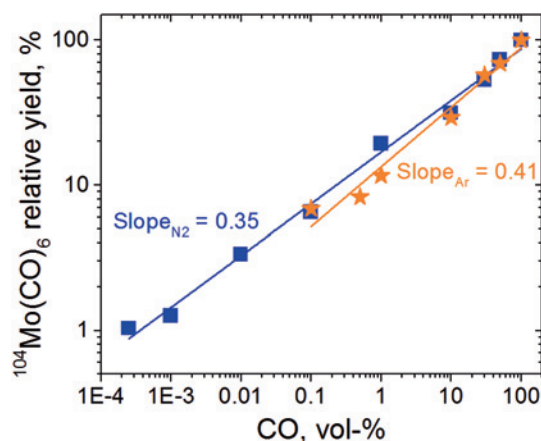
Figure 4: The dependence of the relative production yield of $^{104}Mo(CO)_6$ on the CO content in the carrier gas (N_2 (■) and Ar (★)) at 1.2 bar and a gas flow rate of 1 L/min. The yields are given relative to the maximum observed production rate at 100% CO content.

by gradually increasing/decreasing the temperature of the furnace and analyzing in real time the corresponding activity of short-lived nuclides reaching the charcoal trap or the COMPACT detector. The respective temperature profiles over the decomposition column were determined for every plateau temperature, as this information is essential for describing the decomposition process (see [13]). The metal decomposition columns were pre-cleaned before each experiment by heating them up to 500 °C in a CO containing gas mixture before use.

2.5 Chemicals and materials

Commercially available gases (CarbaGas) Ar (5.0, i.e. purity ≥99.9990%), N_2 (5.0), CO (4.7), He (6.0), CO_2 (4.8), O_2 (5.0) were used without further purification. Metal foils (Goodfellow) were pre-cleaned before use with acetone and ethanol (both VWR). The purity of the carrier gas in the system was monitored by a quadrupole mass-spectrometer with atmospheric pressure inlet (MKS Cirrus 2® Atmospheric QMS), connected directly behind the decomposition column (see Sections 3.7 and 3.8).

3 Results and discussion

3.1 Maximization of the production yield

One of the most important issues in chemical studies of SHE is an optimization of the production yield of the desired compound. Therefore, the influence of the CO con-

tent, the gas flow rate, and the pressure in the recoil chamber on the production yield of $Mo(CO)_6$ have been examined.

The production yield of $^{104}Mo(CO)_6$ strongly depends on the CO concentration in the carrier gas [16]. Thermalization of the fission product in CO-rich gas mixtures allows for significantly higher production yields of $^{104}Mo(CO)_6$ (Figure 4) compared to carrier gases with lower CO content. The ^{104}Mo is produced in ultra-trace amounts (around 10^4 atoms per second), hence even a few ppm of CO in the carrier gas provide orders of magnitude excess of CO in comparison to Mo. Nevertheless, a positive correlation between the CO content and the production yield is observed. No formation of volatile complexes was detected, if SF-fragments were thermalized in pure N_2. In this case, the produced Mo atoms either diffuse to the walls of the recoil chamber, where they irreversibly adsorb, or they are flushed out of the chamber and are retained on the surface of the outlet capillary.

The stopping power [25] of the carrier gas has to be taken into account when the effect of the CO concentration on the production yield of $Mo(CO)_6$ is investigated. If the recoiling Mo atom is thermalized too close to the surface of the SF-source or too close to the outlet capillary, formation of the hexacarbonyl complex might be suppressed. This effect depends on the reaction time and the flow pattern of the gas inside the chamber. However, in case of different CO/N_2 mixtures, the effect of a change of the stopping range of the recoiling atoms is negligible due to a similar stopping power of N_2 and CO for the fission products [26].

If we assume that the amount of the $^{104}Mo(CO)_6$ transported to the charcoal is proportional to the reaction
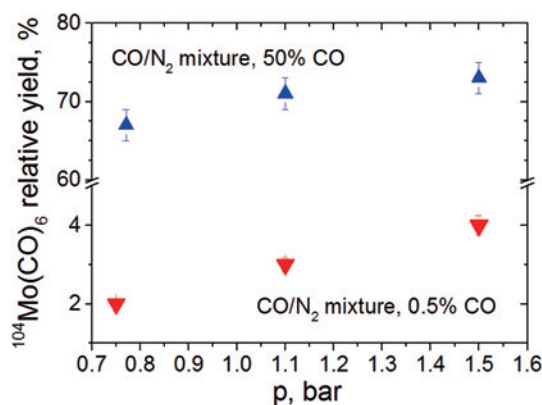
Figure 5: Influence of the pressure in the "Ms. Piggy" recoil chamber on the relative production yield of $Mo(CO)_6$. The yields are given relative to the maximum observed production rate at 100% CO content.

Figure 6: Influence of the CO concentration in the CO/N_2 carrier gas mixture at different gas flow rates on the production yield of $^{104}Mo(CO)_6$, the pressure was kept constant at 1.2 bar. The yields are given relative to the maximum observed production rate at 100% CO content and 1.5 L/min gas flow rate.

rate (Eq. (1)), then the reaction order with respect to CO can be determined by plotting logarithmically the production yield versus the CO content. The slope of the obtained dependence provides the desired reaction order for CO (Figure 4). The slope was found to be slightly dependent on the diluting gas, but remained clearly below first order over a large concentration range. The first-order reaction was expected, since step by step addition of CO to the central atom is assumed to be the most probable reaction path according to the collision theory.

$$^{104}Mo + 6CO \rightarrow Mo(CO)_6 \qquad (1)$$
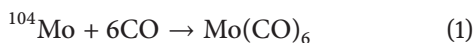
The pressure in the recoil chamber is likewise in a positive correlation with the observed production yield of $^{104}Mo(CO)_6$ (Figure 5). At a fixed gas flow rate, higher pressure increases the production yield due to the growing probability of interaction between Mo and CO molecules in the carrier gas. Additionally, diffusion to the walls of the recoil chamber is slowed down at higher pressures, thereby promoting the formation of the complex as well.

Increasing gas flow rates cause higher transported yields over a wide range of CO concentrations (Figure 6), because faster transport leads to smaller losses due to radioactive decay. However this cannot explain the observed differences for ^{104}Mo with a mean lifetime of 87 s: the 83 ml volume of the recoil chamber together with the volume of the transport tubing of 1.75 m length and an inner diameter of 2 mm corresponds to a transport time of only 9 s at 0.7 L/min gas flow rate, assuming plug flow and a full volume exchange. Therefore, there must be other factors contributing to the significant decrease of the transport yield at lower gas flow rates. To clarify the observed dependence, flow patterns of the carrier gas inside the
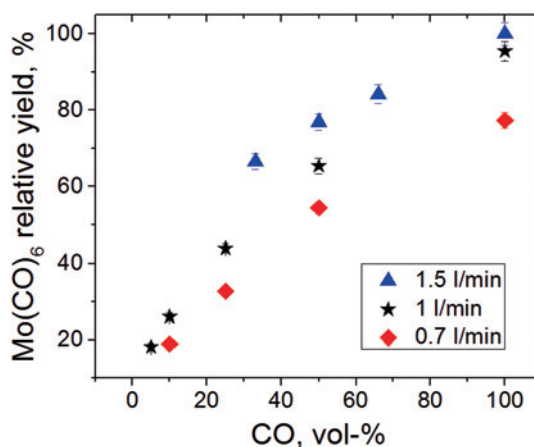
"Ms. Piggy" recoil chamber were simulated using the COM-SOL Multiphysics® software package. The stopping range of ^{104}Mo, recoiling from the ^{252}Cf SF-source with an energy of 110 MeV, was estimated to be around 28 mm in pure CO [26]. This estimation included the 6 μm Al foil, covering the ^{252}Cf source [14]. Thus the initial distribution of Mo inside the chamber was simulated as a spherical dome with a radius of 28 mm. According to these simulations, slightly more than 97% of ^{104}Mo is transported out of the chamber within 10 sec at the experimentally established gas flow rates (Figure 6). This implies that the dead volume in the chamber does not affect the transport efficiency significantly. Nevertheless, Figure 6 suggests that the transport of ^{104}Mo out of the chamber is more efficient at 1.5 L/min, compared to 0.7 L/min or 1.0 L/min.

The adsorption enthalpy of $Mo(CO)_6$ on quartz is determined to be -50 ± 2 kJ/mol [9]. Although this value hints towards weak interaction between the molecule and the surface, the adsorption time of $Mo(CO)_6$ in the typically long PFA Teflon® capillary, connecting the recoil chamber and the charcoal trap, cannot be neglected at ambient conditions. By using a microscopic Monte-Carlo based model [27], we estimated the average time $Mo(CO)_6$ spends adsorbed on the surface of PFA Teflon® tubing on its way to the charcoal trap, using a 4 kJ/mol lower adsorption enthalpy as compared to SiO_2 [28]. At 0.7 L/min this time amounts to 20 sec, while at 1.5 L/min it is approaching 10 sec. Thus the adsorption of carbonyl complexes on the surface of the transport capillaries seems to be the main contributor to the observed differences and might cause significant losses when experiments with short-lived isotopes are performed.

Furthermore, we changed the material of the target chamber from aluminum to the more inert PFA Teflon®. No significant change of the overall measured $^{104}Mo(CO)_6$ yield was observed, pointing to a similar stability of this compound in contact with both surfaces at room temperature. Finally, the replacement of all steel surfaces by polyethylene increased the overall activity of all transported species detected on the charcoal trap, indicating an enhanced retention or even decomposition of carbonyl complexes on steel. This effect, however, was not quantified.

3.2 Material for the decomposition column

For a fast and efficient examination of the stability of carbonyl complexes, we implemented a *tubular flow reactor* (*decomposition column*), with adjustable wall temperature and variable surface material. The length of the column was chosen as 1 m, so that every transported molecule had several chances to interact with the surface material at the chosen gas flow rates even at the highest used temperatures [27]. The final outcome of a decomposition experiment is a *decomposition curve*, which represents the survival probability of the compound at a given temperature in the *tubular flow reactor*.

Different materials were tested in order to identify the optimum surface for the decomposition studies (Figure 7). A freshly pre-cleaned gold surface decomposes 40% of the transported $Mo(CO)_6$ already at room temperature. PFA Teflon®, in contrast, is very inert towards carbonyl complexes; no decomposition was observed up to 300 °C. Unlike Ag and quartz, Pd has a strong affinity
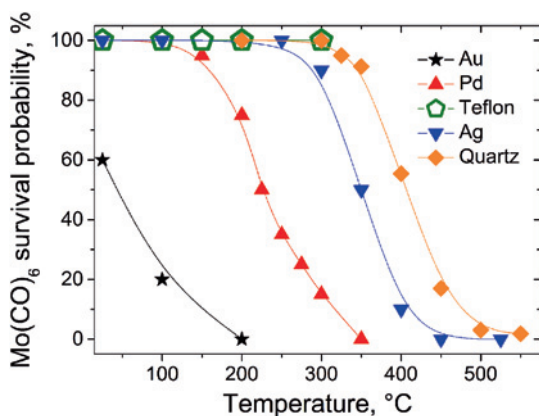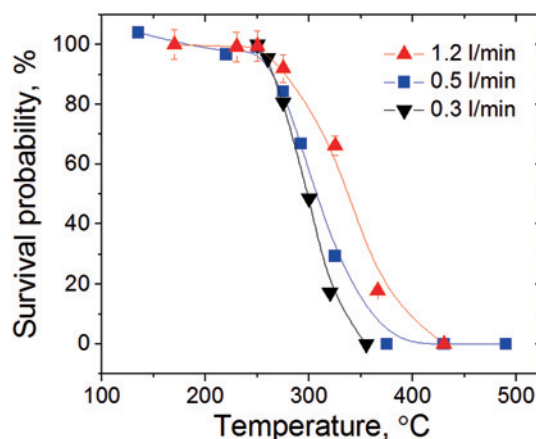
to CO, $-\Delta H_{ads}(CO) = 142-167\,kJ/mol$ [29], which facilitates the decomposition of carbonyls, and thus complicates the modelling of the process. So the choice of the surface for the decomposition was narrowed down to Ag and quartz, both of which show only a weak CO adsorption interaction [30, 31]. The possibility of unidentified side reactions on the hydroxylated quartz surface upon the decomposition of carbonyl complexes, as reported in [32], precluded the use of quartz. Thus, we chose Ag surfaces for further decomposition studies of group 6 carbonyl complexes.

3.3 Decomposition of $^{104}Mo(CO)_6$

The shape and the position of a decomposition curve depend on the investigated complex and on the applied experimental conditions. By increasing the gas flow rate, the average time the complex spends in the tubular flow reactor decreases, and therefore a higher temperature is needed for a complete decomposition (Figure 8) pointing towards a several-chance-process, i.e., even at high temperatures not every surface encounter leads to decomposition. A significant change of the CO content in the carrier gas affects the decomposition rate as well [33], which provides an indication, that low CO contents (few vol-%) suppress reversible decomposition in the gas phase. High CO concentrations favor the reversibility of this homogeneous Mo-CO bond dissociation, due to a higher probability of the back reaction, thereby shifting the decomposition curves towards higher temperatures. The heterogeneous decomposition reaction on the hot silver surface
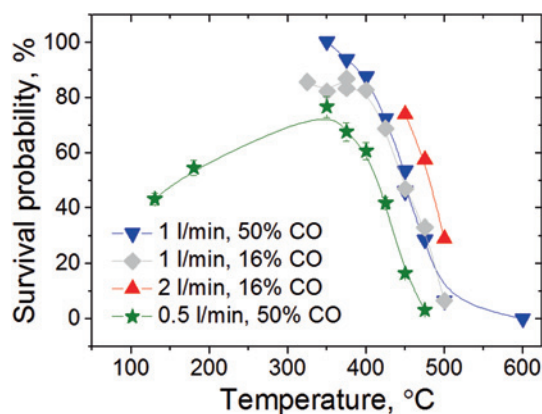

Figure 7: $^{104}Mo(CO)_6$ decomposition curves on different surfaces at otherwise identical experimental conditions. The *x*-axis temperatures correspond to the *plateau temperatures* of the furnace (see Figure 3).

Figure 8: $^{104}Mo(CO)_6$ decomposition curves obtained at 1.2 L/min, 0.5 L/min and 0.3 L/min gas flow rates on a silver surface. The CO concentration was kept constant at 16 vol-%, $p = 1.2$ bar. Lines are shown to guide the eye. The temperatures given on the *x*-axis refer to the *plateau temperatures* of the furnace (see Figure 3).

is considered to be irreversible regardless of the CO content, as the formation of a strong bond between Ag and Mo can be expected [34, 35]. Finally, independent of the applied gas flow rate and its composition, the decomposition reaction of ^{104}Mo(CO)$_6$ starts on silver consistently at a *plateau temperature* of 250 °C (see Figure 8).

3.4 Decomposition studies with ^{87,88}Mo(CO)$_6$ and ^{163,164}W(CO)$_6$

In the case of ^{163,164}W(CO)$_6$, on-line alpha-particle spectroscopy of the adsorbed and the in-flight decaying complexes [9] allowed for quantitative assessment of the production and the decomposition processes. Four breakthrough decomposition curves were measured at different experimental conditions (Figure 9). In agreement with what was previously determined with ^{104}Mo(CO)$_6$, higher flow rates of the carrier gas shift the decomposition curves to higher temperatures also for W(CO)$_6$. Decreasing the CO content from 50 to 16 vol-% did not show a significant impact on the decomposition behavior of W(CO)$_6$, supporting the assumption of a preferred heterogeneous decomposition at the chosen high CO concentrations. Surprisingly, at 0.5 L/min gas flow rate (Figure 9, ★), the decomposition curve did not recover to 100% survival probability even at low temperatures. A similar behavior was observed when the break-through curve of ^{87,88}Mo(CO)$_6$ was measured at 0.5 L/min gas flow rate and 50 vol-% CO concentration in the carrier gas (Figure 10). This issue is currently under further investigation. Regardless of the experimental parameters, the decomposition reaction of W(CO)$_6$ starts consistently at around 350 °C, which is
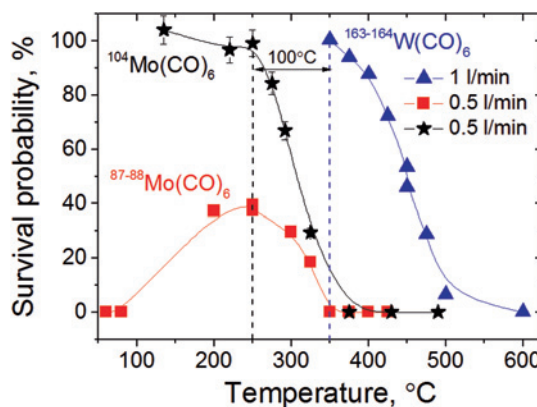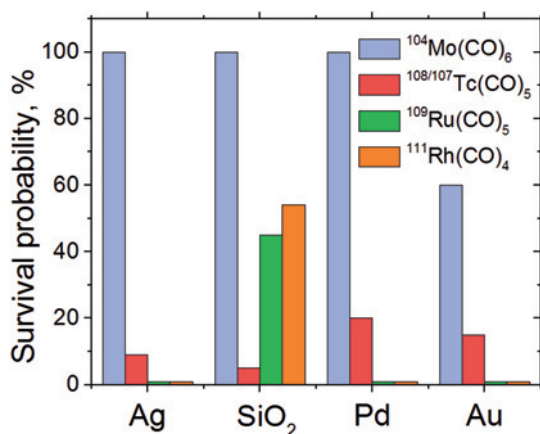
Figure 10: Decomposition curves of Mo and W carbonyl complexes on a silver surface. The CO concentration was kept constant at 50 vol-%. Lines are given to guide the eye. The temperatures given on the *x*-axis refer to the *plateau temperatures* of the furnace (see Figure 3).

100 °C higher, compared to Mo(CO)$_6$ (Figure 10). Therefore, we conclude that a difference in the first bond dissociation energies of 23 kJ/mol [1] leads to a 100 °C shift in the decomposition temperature. The half-life dependence of the decomposition can be neglected, since a by-pass column of the same volume was used to establish the relative 100% value of produced and transported species.

3.5 Tc, Rh and Ru carbonyl complexes

Apart from Mo, there are three other elements present in the recoil chamber of "Ms. Piggy", which form carbonyl complexes at ambient conditions [16, 17, 44]. The formation of polyatomic clusters between the central atoms (e.g. Tc$_2$(CO)$_{10}$) is precluded in our studies due to only ultra-trace amounts of these elements being present in the recoil chamber. The formation of polyatomic clusters between the central atoms (e.g. Tc$_2$(CO)$_{10}$) is precluded in our studies due to only ultra-trace amounts of these elements being present in the recoil chamber. The 18-electron rule suggests for complexes of Tc, Ru, and Rh with single central atoms the following composition with the maximum number of CO ligands: Tc(CO)$_5$, Ru(CO)$_5$, Rh(CO)$_4$. The stability of a complex of any given isotope can be monitored accurately only if its parent nuclide is not forming volatile complexes and thus is not being transported to the charcoal trap, or if the half-life of the parent nuclide is too short for an effective transport. Therefore, properties of the formed complexes were monitored in separate isobars so that the precursor effects [28] could be excluded.

In contrast to Mo(CO)$_6$, carbonyl complexes of Tc, Ru and Rh were found to be readily decomposing on various

Figure 9: $^{163-164}$W(CO)$_6$ decomposition curves on a silver surface at different experimental conditions. Lines are shown to guide the eye. The temperatures given on the *x*-axis refer to the *plateau temperatures* of the furnace (see Figure 3).

Figure 11: Stability of Mo, Tc, Ru and Rh carbonyl complexes at temperatures close to ambient (30–50 °C) in contact with different surfaces.

Table 1: Activity ratio between Mo and Tc, determined in the 6 m long tube, wrapped around the HPGe γ-ray detector head. Statistical error limits are given at the 68% confidence interval.

Isobar	104		105	
Element	Mo	Tc	Mo	Tc
Half-life, s	60	1092	35.6	456
Activity ratio	0.9 ± 0.1		0.9 ± 0.1	

surfaces even at temperatures close to ambient (Figure 11). The observed behavior supports thermochromatographic studies with $Tc(CO)_5$ on gold surfaces [36], where an unexpectedly high affinity of the complex to the Au surface was determined. The decomposition behavior of Ir and Re carbonyl complexes reported in [17] seems to be in contradiction with our findings. Being homologues of Tc and Rh, these complexes are expected to have similar chemical properties. However, both volatile carbonyl complexes of Re and Ir were found to be stable up to 200 °C on the quartz surface. Whether this is indicative of increasing stability when going from the lighter to the heavier members of groups 7 and 9, or is due to minor, but potentially important differences between our studies and those reported in [17] is currently not clear.

3.6 β^--decay and formation of $Tc(CO)_5$

β^--decay of ^{99}Mo in the form of hexacarbonyl, followed by the formation of $^{99m}Tc(CO)_5$, was reported in [37]. We intended to investigate the similar reaction to see whether the formation of carbonyl complexes is possible outside of the "Ms. Piggy" recoil chamber as well. For this, the charcoal trap in our setup (Figure 2) was replaced by a 6 m long PFA Teflon® tube, wrapped around the HPGe detector head. At 0.5 L/min gas flow rate the average transport time through this tube was around 9 s for complete volume exchange not considering adsorption retention. Pure CO was used as a carrier gas.

The maximum energy of the emitted β^--particle is much higher for ^{104}Mo and ^{105}Mo, compared to ^{99}Mo. Thus, the energy of the activated state of Tc must be high enough for entering the reaction path with CO. However,

if the reaction time is longer than the time required for the diffusion of the formed atom to the nearest wall, irreversible adsorption of Tc will happen and no complex will be formed. The PFA Teflon® tube had an inner diameter of 4 mm. Hence, the average time for ^{105}Tc to diffuse over 2 mm distance was estimated to be about 0.1 s at ambient conditions. Gilliland's empirical equation [38] has been applied to estimate the ^{104,105}Tc diffusion coefficient. Thus, we conclude from the non-transport of Tc that the reaction time between Tc and CO in the gas phase must exceed 0.1 s. This time includes also the deexcitation of the recoiling ion, which is supposed to be in the microsecond time scale at maximum in a gas at atmospheric pressure [39].

3.7 Influence of carbon dioxide

Due to relatively high sublimation point (−78 °C), carbon dioxide freezes in the COMPACT detector. If macroscopic amounts are present, this will block the detector channel and deteriorate the energy resolution of the alpha-particle spectroscopy. CO_2 is present as a trace impurity in commercially available carbon monoxide and can also be permanently produced by oxidation of the latter in the gas-jet system by trace contaminations with oxygen and water. Thus special cleaning units such as molecular sieves, liquid nitrogen traps, or chemical absorbents have to be employed in the system for effective elimination of CO_2. Implementation of a decomposition column facilitates the reaction between CO and O_2 and therefore promotes the formation of CO_2 in the system. The operation of a silver column at 500 °C brings about a twofold increase in the CO_2 content, as determined with MKS Cirrus 2® atmospheric pressure mass spectrometer (see Figure 12). This particular source of CO_2 cannot be easily eliminated, because cleaning units between the recoil chamber and the detection system cannot be installed. Therefore, the carrier gas must be efficiently pre-cleaned with respect to CO_2 and O_2 admixtures before use, and kept clean.
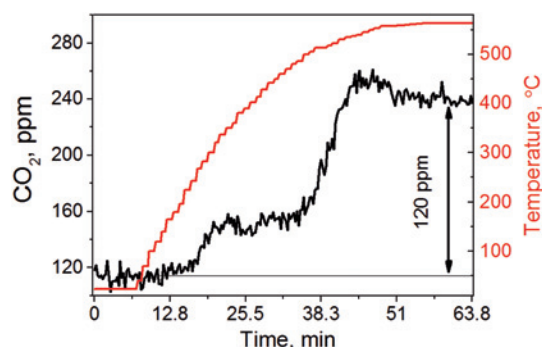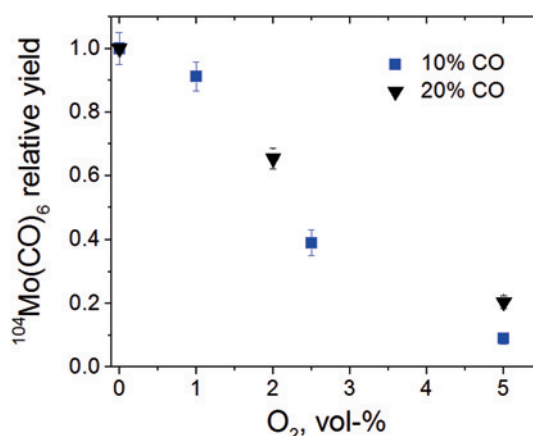
Figure 12: Influence of the silver decomposition column temperature on the CO_2 content in the carrier gas at 1 L/min gas flow rate and 100 vol-% CO content.

Figure 13: Influence of the O_2 content in the carrier gas (CO/N_2) on the $^{104}Mo(CO)_6$ production yield. The gas flow rate and the pressure were kept constant at 1 L/min and 1.2 bar respectively. Statistical error limits are given at the 68% confidence level. The yields are given relative to the maximum observed production rate at the given experimental conditions.

3.8 Influence of oxygen

O_2 has a strong impact on the production yield of $^{104}Mo(CO)_6$ (Figure 13). Few vol-% of O_2 in the carrier gas caused the *relative yield* to drop to less than 25%. The effect is attributed to the high stability of Mo oxides. The formation enthalpies of MoO_2 and MoO_3 are -589 kJ/mol and -745 kJ/mol, respectively [40], while the formation of $Mo(CO)_6$ from Mo and CO corresponds to -320 kJ/mol [41] only. We did not study the influence of oxygen content on the production yields of $W(CO)_6$ so far. Nevertheless, it was qualitatively observed that the formation of $W(CO)_6$ is much more sensitive to O_2, than the formation of $Mo(CO)_6$, by comparing transport yields of the carbonyl complexes of both elements with and without Oxysorb® cartridges installed in the gas-loop described in [9]. This can be attributed to an even higher stability of WO_2 and WO_3, which have formation enthalpies of -590 kJ/mol and -843 kJ/mol, respectively [42]. SgO_3 was predicted to have a heat of formation between -874 kJ/mol and -951 kJ/mol [43], which makes this system the most sensitive to O_2 among all group 6 elements.

4 Summary and conclusions

We suggest a fast and efficient approach for testing the stability of the group 6 carbonyl complexes. The implementation of a tubular flow reactor has proven to be efficient in differentiating between the thermal stabilities of $Mo(CO)_6$ and $W(CO)_6$, having a 23 kJ/mol difference in their first bond dissociation energies. Therefore, we conclude that a future experiment with $Sg(CO)_6$ seems feasible with the developed setup. Such an experiment will

benchmark the predicted hexacarbonyl stability sequence in group 6 of the periodic table.

Silver was determined to be the most appropriate surface for the decomposition studies of the group 6 carbonyl complexes. In contrast, due to the high decomposition rate of the Tc-carbonyl complex, $Ru(CO)_5$, and Rh-carbonyl complex already at ambient conditions, precludes Ag surface from being used for assessing their stabilities. Thus, the search for other materials or another approach is necessary, if stability tests of potential carbonyl compounds of Bh, Hs or Mt are envisaged.

We optimized the production rate of $Mo(CO)_6$ under conditions relevant for a future experiment with Sg. In order to maximize the yield of the Sg carbonyl complex, CO concentration, pressure in the RTC, and the carrier gas flow rate are ideally kept as high as possible. The retention of carbonyl complexes on Teflon® and other surfaces present in the gas loop has to be considered for optimizing the transport efficiency. The oxygen content should be minimized and constantly monitored, as Sg oxides are predicted to be even more stable than oxides of W and Mo. Furthermore, O_2 was found to oxidize CO in the decomposition column, which has detrimental effects on the gas-jet transport system and on the cryo-thermochromatography on-line detection unit in particular.

From our investigations on the formation of $^{104,105}Tc$ carbonyl complexes from β^--decaying $^{104,105}Mo(CO)_6$ precursors, we conclude that the lower limit for the reaction time between the Tc atom and CO is around 100 ms. Finally, the obtained results on the decomposition of group 6 carbonyls allowed for the design and test of

a decomposition model which relates the experimental observations to thermochemical stability data available for the carbonyl compounds. This data evaluation is described in [13].

References

1. Lewis, K. E., Golden, D. M., Smith, G. P.: Organometallic Bond Dissociation Energies: Laser Pyrolysis of $Fe(CO)_5$, $Cr(CO)_6$, $Mo(CO)_6$, and $W(CO)_6$. J. Am. Chem. Soc. **106**, 3905–3912 (1984).

2. Schädel, M., Shaughnessy, D.: Chemistry of superheavy elements. Second Edition, Springer (2014).

3. Türler, A., Pershina, V.: Advances in the production and chemistry of the heaviest elements. Chem. Rev. **113**, 1237–312 (2013).

4. Schädel, M.: Chemistry of superheavy elements. Radiochim. Acta. **100**, 579–604 (2012).

5. Schädel, M.: Chemistry of superheavy elements. *Angew. Chemie* **45**, 368–401 (2006).

6. Eichler, R., Aksenov, N. V., Albin, Y. V., Belozerov, A. V., Bozhikov, G. A., Chepigin, V. I., Dmitriev, S. N., Dressler, R., Gäggeler, H. W., Gorshkov, V. A., Henderson, G. S.: Indication for a volatile element 114. Radiochim. Acta **98**, 133–139 (2010).

7. Eichler, R., Aksenov, N. V., Belozerov, A. V., Bozhikov, G. A., Chepigin, V. I., Dmitriev, S. N., Dressler, R., Gäggeler, H. W., Gorshkov, V. A., Haenssler, F., Itkis, M. G., Laube, A., Lebedev, V. Y., Malyshev, O. N., Oganessian, Y. T., Petrushkin, O. V., Piguet, D., Rasmussen, P., Shishkin, S. V., Shutov, A. V., Svirikhin, A. I., Tereshatov, E. E., Vostokin, G. K., Wegrzecki, M., Yeremin, A. V.: Chemical characterization of element 112. Nature **447**, 72–75 (2007).

8. Yakushev, A., Gates, J. M., Türler, A., Schädel, M., Düllmann, Ch. E., Ackermann, D., Andersson, L.-L., Block, M., Brüchle, W., Dvorak, J., Eberhardt, K., Essel, H. G., Even, J., Forsberg, U., Gorshkov, A., Graeger, R., Gregorich, K. E., Hartmann, W., Herzberg, R.-D., Heßberger, F. P., Hild, D., Hübner, A., Jäger, E., Khuyagbaatar, J., Kindler, B., Kratz, J. V., Krier, J., Kurz, N., Lommel, B., Niewisch, L. J., Nitsche, H., Omtvedt, J. P., Parr, E., Qin, Z., Rudolph, D., Runke, J., Schausten, B., Schimpf, E., Semchenkov, A., Steiner, J., Thörle-Pospiech, P., Uusitalo, J., Wegrzecki, M., Wiehl, N.: Superheavy element flerovium (element 114) is a volatile metal. Inorg. Chem. **53**, 1624–1629 (2014).

9. Even, J., Yakushev, A., Düllmann, Ch. E., Haba, H., Asai, M., Sato, T. K., Brand, H., Di Nitto, A., Eichler, R., Fan, F. L., Hartmann, W., Huang, M., Jäger, E., Kaji, D., Kanaya, J., Kaneya, Y., Khuyagbaatar, J., Kindler, B., Kratz, J. V., Krier, J., Kudou, Y., Kurz, N., Lommel, B., Miyashita, S., Morimoto, K., Morita, K., Murakami, M., Nagame, Y., Nitsche, H., Ooe, K., Qin, Z., Schädel, M., Steiner, J., Sumita, T., Takeyama, M., Tanaka, K., Toyoshima, A., Tsukada, K., Türler, A., Usoltsev, I., Wakabayashi, Y., Wang, Y., Wiehl, N., Yamaki, S.: Synthesis and detection of a seaborgium carbonyl complex Science **345**, 1491–1493 (2014).

10. Pershina, V., Anton, J.: Theoretical predictions of properties and gas-phase chromatography behaviour of carbonyl complexes of group-6 elements Cr, Mo, W, and element 106, seaborgium. J. Chem. Phys. **138**, 174301–6 (2013).

11. Pyykkö, P.: Relativistic Effects in Structural Chemistry. Chem. Rev. **88**, 563–594 (1988).

12. Nash, C. S., Bursten, B. E.: Prediction of the bond lengths, vibrational frequencies, and bond dissociation energy of octahedral seaborgium hexacarbonyl, $Sg(CO)_6$. J. Am. Chem. Soc. **121**, 10830–10831 (1999).

13. Usoltsev, I., Eichler, R., Türler, A.: Decomposition Studies of the Group VI Hexacarbonyls Complexes. Part 2: Modelling of the Decomposition Process. In preparation.

14. Düllmann, Ch. E., Eichler, B., Eichler, R., Gäggeler, H. W., Jost, D. T., Kindler, U., Piguet, D., Soverna, S., Thörle, P., Trautmann, N., Türler, A.: Miss Piggy, a californium-252 fission fragment source as a generator of short-lived radionuclides. Nucl. Instr. and Meth. A **512**, 595–605 (2003).

15. Blachot, J.: Nuclear Data Sheets for $A = 104$. *Nucl. Data Sheets* **108**, 2035–2172 (2007).

16. Even, J., Yakushev, A., Düllmann, Ch.E., Dvorak, J., Eichler, R., Gothe, O., Hild, D., Jäger, E., Khuyagbaatar, J., Kratz, J. V., Krier, J., Niewisch, L., Nitsche, H., Pysmenetska, I., Schädel, M., Schausten, B., Türler, A., Wiehl, N., Wittwer, D.: Rapid synthesis of radioactive transition-metal carbonyl complexes at ambient conditions. Inorg. Chem. **51**, 6431–6433 (2012).

17. Even, J., Yakushev, A., Düllmann, Ch. E., Dvorak, J., Eichler, R., Gothe, O., Hartmann, W., Hild, D., Jäger, E., Khuyagbaatar, J., Kindler, B., Kratz, J. V., Krier, J., Lommel, B., Niewisch, L., Nitsche, H., Pysmenetska, I., Schädel, M., Schausten, B., Türler, A., Wiehl, N., Wittwer, D.: In-situ formation, thermal decomposition, and adsorption studies of transition metal carbonyl complexes with short-lived radioisotopes. Radiochim. Acta **102**, 1093–1110 (2014).

18. Morita, K., Yoshida, A., Inamura, T. T., Koizumi, M., Nomura, T., Fujioka, M., Shinozuka, T., Miyatake, H., Sueki, K., Kudo, H.,

Nagai, Y., Toriyama, T., Yoshimura, K., Hatsukawa, Y.: RIKEN isotope separator on-line GARIS/IGISOL. Nucl. Instr. and Meth. B **70**, 220–225 (1992).

19. Reich, C. W.: Nuclear Data Sheets for $A = 159$. Nucl. Data Sheets **113**, 157–363 (2012).

20. Reich, C. W.: Nuclear Data Sheets for $A = 160$. Nucl. Data Sheets **105**, 557–774 (2005).

21. Helmer, R. G.: Nuclear Data Sheets for $A = 87$. Nucl. Data Sheets **95**, 543–678 (2002).

22. McCutchan, E. A., Sonzogni, A. A.: Nuclear Data Sheets for A = 88. Nucl. Data Sheets **115**, 135–304 (2014).

23. Dvorak, J., Brüchle, W., Chelnokov, M., Dressler, R., Düllmann, Ch. E., Eberhardt, K., Gorshkov, V., Jäger, E., Krücken, R., Kuznetsov, A., Nagame, Y., Nebel, F., Novackova, Z., Qin, Z., Schädel, M., Schausten, B., Schimpf, E., Semchenkov, A., Thörle, P., Türler, A., Wegrzecki, M.,Wierczinski, B., Yakushev, A., Yeremin, A.: Doubly Magic Nucleus (108)(270)Hs(162). Phys. Rev. Lett. **97**, 242501 (2006).

24. Even, J., Ackermann, D., Asai, M., Block, M., Brand, H., Di Nitto, A., Düllmann, Ch. E., Eichler, R., Fan, F. L., Haba, H., Hartmann, W., Hübner, A., Heßberger, F. P., Huang, M., Jäger, E., Kaji, D., Kanaya, J., Kaneya, Y., Khuyagbaatar, J., Kindler, B., Kratz, J. V., Krier, J., Kudou, Y., Kurz, N., Laatiaoui, M., Lommel, B., Maurer, J., Miyashita, S., Morimoto, K., Morita, K., Murakami, M., Nagame, Y., Nitsche, H., Ooe, K., Qin, Z., Sato, T. K., Schädel, M., Steiner, J., Sumita, T., Takeyama, M., Tanaka, K., Toyoshima, A., Tsukada, K., Türler, A., Usoltsev, I., Wakabayashi, Y., Wang, Y., Wiehl, N., Yakushev, A., Yamaki, S.: In situ synthesis of volatile carbonyl complexes with short-lived nuclides. J. Radioanal. Nucl. Chem. **303**, 2457–2466 (2015).

25. Forte, M., Bertin, A., Bruno, M., Vannini, G., Vitale, A.: Experimental study on the energy loss in argon of Cf-252 fission fragments. Phys. Rev. B **14**,956–968 (1976).

26. Ziegler, J. F., Ziegler, M. D., Biersack, J. P.: SRIM – The stopping and range of ions in matter (2010) Nucl. Instr. and Meth. B **268**, 1818–1823 (2010).

27. Zvara, I.: Simulation of thermochromatographic processes by the Monte Carlo method. Radiochim. Acta **1**, 95–102 (1985).

28. Wang, Y., Qin, Z., Fan, F. L., Fan, F. Y., Cao, S. W., Wu, X. L., Zhang, X., Bai, J., Yin, X. J., Tian, L. L., Zhao, L., Tian, W., Li, Z., Tan, C. M., Guo, J. S., Gäggeler, H. W.: Gas-phase chemistry of Mo, Ru, W, and Os metal carbonyl complexes. Radiochim. Acta **102**, 69–76 (2014).

29. Conrad, H., Ertl, G., Koch, J., Latta, E. E.: Adsorption of CO on Pd single crystal surfaces. Surf. Science **43**, 462–480 (1974).

30. McElhiney, G., Papp, H., Pritchard, J.: The adsorption of Xe and CO on Ag(111). Surf. Science **54**, 617–634 (1976).

31. Beebe, T. P., Gelin, P., Yates, J. T., Infrared spectroscopic observations of surface bonding in physical adsorption: The physical adsorption of CO on SiO_2 surfaces. Surf. Science **148**, 526–550 (1984).

32. Phillips, J., Dumestic, J.: Production of supported metal catalysts by the decomposition of metal carbonyls. Appl. Catal. **9**, 1–30 (1984).

33. Usoltsev, I., Eichler, R., Piguet, D., Wang, Y., Qin, Z., Türler, A.: Formation and stabilization of a molybdenum dinitrogen carbonyl complex at ambient. In preparation.

34. Eichler, B., Rossbach, H.: Adsorption of volatile metals on metal surfaces and its application in nuclear chemistry. Radiochim. Acta **33**, 121–125 (1983).

35. Eichler, B.: Report ZfK – 396. 1979.

36. Even, J.: Developments for transactinide chemistry experiments behind the gas-filled separator TASCA. Ph.D. Thesis, University of Mainz, Germany (2011).

37. De Jong, I. G., Wiles, D. R.: Studies on the Pentacarbonyltechnetium Radical. Inorg. Chem. **12**, 5–8 (1973).

38. Chen, N., Othmer, D.: New generalized equation for gas diffusion coefficient. J. Chem. Eng. Data **7**, 37–41 (1962).

39. Jeong, J. Y., Babayan, S. E., Tu, V. J., Park, J., Henins, I., Hicks, R. F., Selwyn, G. S.: Etching materials with an atmospheric-pressure plasma jet. Plasma Sources Sci. Technol. **7**, 282–285 (1998).

40. Staskiewicz, B. A., Tucker, J. R., Snyder, P. E.: The Heat of Formation of Molybdenum Dioxide and Molybdenum Trioxide. J. Am. Chem. Soc. **6**, 2987–2989 (1955).

41. Cotton, F., Fischer, A., Wilkinson, G.: Heats of Combustion and Formation of Metal Carbonyls. I. Chromium, Molybdenum and Tungsten Hexacarbonyls. J. Am. Chem. Soc. **78**, 5168–5171 (1956).

42. Mah, A.: The heats of formation of tungsten trioxide and tungsten dioxide. J. Am. Chem. Soc. **81**, 4–5 (1959).

43. Eichler, B., Türler, A., Gäggeler, H. W.: Thermochemical characterization of seaborgium compounds in gas adsorption chromatography. J. Phys. Chem. A **103**, 9296–9306 (1999).

44. Wang, Y., Qin, Z., Fan, F.-L., Haba, H., Komori, Y., Cao, S.-W., Wua, X.-L., Tana, C.-M.: Gas-phase chemistry of technetium carbonyl Complexes. Phys. Chem. Chem. Phys. **17**, 13228–13234 (2015).